TATA-Binding Protein Recognition and Bending of a Consensus Promoter Are Protein Species Dependent[†]

JoDell E. Whittington,[‡] Roberto F. Delgadillo,[‡] Torrissa J. Attebury,[‡] Laura K. Parkhurst,[‡] Margaret A. Daugherty,[§] and Lawrence J. Parkhurst*,[‡]

Department of Chemistry, University of Nebraska—Lincoln, Lincoln, Nebraska 68588-0304, and Department of Chemistry and Biochemistry, Middlebury College, Middlebury, Vermont 05753

Received January 24, 2008; Revised Manuscript Received April 17, 2008

ABSTRACT: The structure and behavior of full-length human TBP binding the *adenovirus* major late promoter (AdMLP) have been characterized using biophysical methods. The human protein induces a 97° bend in DNA_{AdMLP}. The high-resolution functional data provide a quantitative energetic and kinetic description of the partial reaction sequence as native human TBP binds rapidly to a consensus promoter with high affinity. The reaction proceeds with successive formation of three bound species, all having strongly bent DNA, with the concurrence of binding and bending demonstrated by both fluorescence and anisotropy stopped flow. These results establish the protein species dependence of the TBP−DNA_{AdMLP} structure and recognition mechanism. Additionally, the strong correlation between the DNA bend angle and transcription efficiency demonstrated previously for yeast TBP is shown to extend to human TBP. The heterologous NH_2-terminal domains are the apparent source of the species-specific differences. Together with previous studies the present work establishes that TBP_{wt}−DNA_{TATA} function and structure depend both on the TATA box sequence and on the TBP species.

The interaction between the TATA-binding protein (TBP)[1] and gene promoters is central to transcription by RNA polymerases I, II, and III (*1–3*). TBP binding of the minor groove of specific "TATA box" sequences (TATAa/tAa/t) results in DNA unwinding coupled with helical bending, creating a unique molecular geometry and bringing linearly separated nucleotides into closer proximity. These architectural changes are critical to the successful assembly of the transcription preinitiation complex (PIC). Mutagenesis studies suggest that the TBP−DNA_{TATA} conformation plays a direct role in transcription activation (*4*) and the extent of the helical bend in yeast TBP−DNA_{TATA} complexes is strongly correlated with transcription efficiency both *in vitro* and *in vivo* (*5*).

Crystallographic studies utilizing DNA_{TATA} bound to the COOH-terminal DNA binding domains (CTDs) of *Saccharomyces cerevisiae* (***y***TBP) (*6*) and *Homo sapiens* (***h***TBP) (*7, 8*) or *Arabidopsis thaliana* (***a***TBP) (*9*) yield superimposable structures, independent of differences in either the TATA box sequence (*10*) or the TBP species (*6, 8, 9, 11*). This apparent universality was partially eclipsed by subsequent biochemical (*12, 13*) and biophysical solution studies (*5, 14–17*) utilizing full-length wild-type ***y***TBP, which showed bends ranging from ∼30° to ∼80° depending on the TATA box sequence. Complementary function studies revealed corresponding TATA sequence-dependent differences for ***y***TBP promoter recognition (*15, 16, 18*). These contrasting results revealed the hazards inherent in generalizing from TBP_{CTD}−DNA_{TATA} complexes in crystals to those in solution and incorporating wild-type TBP: the model in which TATA sequences are variably bent over a ∼50° range leads to a significantly different biological view than does one based on universal ∼80° bending.

Although the above-cited studies resolved the promoter sequence dependence of ***y***TBP_{wt}−DNA_{TATA} structure and function, the protein species dependence of the TBP−DNA_{TATA} interaction has remained an open question. Function studies of full-length TBP reported to date have utilized primarily yeast TBP, showing an endothermic reaction (*15,-16, 18, 19*) with simultaneous DNA binding and bending (*18,-20*) and sequential formation of multiple stable ***y***TBP−DNA species having bent DNA (*15, 16, 18*). The extent to which this mechanism can be generalized to other TBP species has been largely a matter of speculation. Additional uncertainty arose from two contradictory models for human TBP−DNA_{AdMLP} binding: one model proposed a low-affinity interaction that included a slow (30 min) isomerization step or TFIIB requirement (*21*), while the other demonstrated broadly shared characteristics for ***h***TBP_{wt} with ***y***TBP_{wt} in that binding was tight, rapid, and concurrent with helical bending (*22*). Establishing the generality or specificity of the TBP-promoter interaction is of special interest since human

[†] The work was supported by NIH Grants GM59346 and RR015468.

* To whom correspondence should be addressed: tel, (402) 472-3316; fax, (402) 472-2044; e-mail, lparkhurst1@unl.edu.

[‡] University of Nebraska—Lincoln.

[§] Middlebury College.

[1] Abbreviations: TBP, TATA-binding protein, with the y and h prefixes denoting yeast and human TBP, respectively; AdMLP, *adenovirus* major late promoter; PIC, preinitiation complex; CTD, COOH-terminal domain; NTD, NH_2-terminal domain; FRET, fluorescence resonance energy transfer; TAMRA, *N*,*N*,*N*′,*N*′-tetramethyl-6-carboxyrhodamine; T*$AdMLP_{dpx}$*F, 14 bp DNA duplex (5′-CGC-TATAAAAGGGC-3′) bearing the eight base AdMLP TATA sequence, with 5′-TAMRA and 3′-fluorescein on the top strand; TFIIA and -B, class II general transcription initiation factors A and B.

10.1021/bi800139w CCC: $40.75
Published on Web 06/14/2008

transcription initiation and regulation are focal points for targeted intervention.

We have thus undertaken a comprehensive biophysical study of the behavior of full-length human TBP with DNA_{AdMLP}. The AdMLP bend angle induced by ***h***TBP_{wt} in solution is shown by time-resolved fluorescence spectroscopy to be significantly larger than that induced by ***y***TBP_{wt}, confirming the TBP species dependence of this key structural feature for $TBP_{wt}-DNA_{AdMLP}$ complexes in solution. High-resolution functional data provide a detailed quantitative description of the partial reaction sequence as ***h***TBP_{wt} binds and bends duplex DNA bearing the AdMLP TATA sequence, with the concurrence of binding and bending demonstrated by combined fluorescence and anisotropy stopped flow. These results establish the TBP species dependence of this process via a clear, reliable, and rigorous comparison of the full-length human and yeast TBPs reactions. Together with published ***y***$TBP-DNA_{TATA}$ studies, these data point to a primary role of the nonconserved TBP NH_2-terminal domains in regulating promoter recognition and subsequent binding of other transcription factors during PIC assembly. Finally, the strong correlation between the degree of the induced DNA_{TATA} bend and relative transcription activity observed previously with ***y***TBP_{wt} (*5*) is shown to extend to ***h***TBP_{wt}.

EXPERIMENTAL PROCEDURES

Our experimental approach combined time-resolved fluorescence resonance energy transfer (FRET), stopped flow FRET, stopped flow anisotropy, binding equilibria, and dissociation kinetics. Detailed discussions of FRET and its application to the present work have been published (*15, 16, 18, 23, 24*). The key practical consideration is that TBP binding and bending of dye-labeled oligomers are directly related to the dramatic changes observed in the fluorescence spectrum of the labeled DNA (Figure 1).

Materials and Solution Conditions. The double and single fluorescently labeled and unlabeled top strands bearing the AdMLP TATA sequence (5′CGC**TATAAAAG**GGC3′) and the corresponding complement were synthesized by TriLink Biotechnologies, Inc. (San Diego, CA) and were identical to those used in our initial ***h***TBP study (*22*) and in previous ***y***$TBP-DNA_{AdMLP}$ studies (*5, 14, 15, 18, 20*). The double fluorescently labeled coding strand is linked through six carbons at the 3′ end to the FRET donor fluorescein and at the 5′ end to the FRET acceptor *N*,*N*,*N*′,*N*′-tetramethyl-6-carboxyrhodamine (TAMRA) and is denoted in the duplex as $T*AdMLP_{dpx}*F$. The corresponding single-labeled strand is identical but without 5′ TAMRA. All labeled strands were both HPLC and PAGE purified. Purity was confirmed by comparing absorbance peak ratios to the corresponding theoretical ratios and considering the dyes' UV contributions. Duplex DNA was prepared using a 10-fold molar excess of complementary strand, shown previously to yield >99% top strand saturation (*25*).

Recombinant full-length human TBP containing only the native amino acid sequence was expressed in *Escherichia coli* and prepared without nonionic detergents as described (*22*) and is monomeric under the solution conditions and concentrations used herein (M. Daugherty, unpublished data). A fluorescence assay similar to that described previously (*22*) was used to determine the protein activity from the limiting

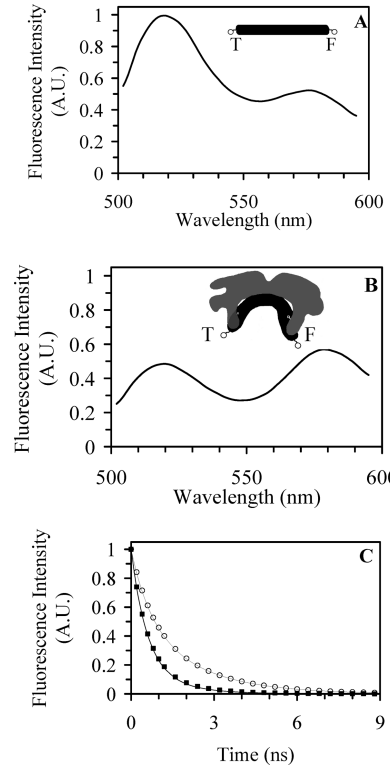

FIGURE 1: Donor fluorescein emission in the steady state (A) and resolved in the ns time regime (C, upper curve) for unbound $T*AdMLP_{dpx}*F$ and the corresponding spectra following human TBP binding (B and C, lower curve). The relatively straight and rigid unbound duplex maintains maximum separation of the 3′ FRET donor, fluorescein (F, 518 nm peak), and the 5′ acceptor, TAMRA (T, 578 nm peak). (A) Since the rate of energy transfer from donor to acceptor depends on the inverse sixth power of the distance between these dyes, the intensity of the fluorescein emission peak is high: the excited state fluorescein population relaxes back to the ground state primarily by photon emission rather than by the transfer of energy to the TAMRA population. (B) ***h***TBP binding and bending result in a much decreased interdye distance, greatly increasing the efficiency of energy transfer and thus decreasing the donor emission. We have shown previously that both the labeled duplex and the protein are stable for at least 1 h under our solution conditions with no measurable change in the spectra over that time period (*22*). (C) The upper decay curve was generated using the free duplex and is the time-resolved counterpart of (A) with a 1.49 ns average donor lifetime. The increased transfer rate following protein-induced bending shortens the lifetime of the observed fluorescein emission (lower curve) to yield the time decay equivalent of (B) and a 0.726 ns average donor lifetime. The protein activity was determined as described to be 26%.

slope of a plot of fractional DNA saturation vs total protein using titration data collected with total DNA $\gg K_d$. The change in fluorescence corresponding to full DNA saturation was determined from the *y*-axis intercept of the reciprocal of the fluorescence change vs the inverse of the total protein concentration.

Experiments were conducted at the temperatures indicated in the same buffer used previously with ***y***TBP_{wt}: 10 mM Tris-HCl, pH 7.4, 100 mM KCl, 2.5 mM $MgCl_2$, 1 mM $CaCl_2$, 5 mM DTT, and 10% glycerol, with 100 mM leupeptin hydrochloride added to enhance protein stability (*22*). The buffer used for measurements in the nanosecond time regime was pH 8 to ensure that fluorescence was from a single fluorescein species (*26*). All TBP concentrations reported are for active protein, and concentrations reported for stopped-flow experiments are given after mixing.

Instrumentation, Data Acquisition, and Analyses. The same procedures and instrumentation used previously with ***y***TBP_{wt} studies (*15, 16, 18*) were intentionally and conscientiously employed in the present study in order to ensure a meaningful comparison between the yeast and human proteins, with a more precise procedure used to determine the value of $\Delta H°$. Steady-state data were collected using a model A-1010 fluorimeter from Photon Technologies, Inc. (Lawrenceville, NJ) with excitation from the 488 nm line of a Coherent model INNOVA 70-4 argon ion laser (Santa Clara, CA). The temperature was held within ±0.05 °C and recorded from a thermistor placed in the temperature-controlled cuvette (Hellma Cells Inc., Plainview, NY). The T*AdMLP$_{dpx}$*F emission spectrum, both free and TBP bound, was confirmed to be invariant over the experimental temperature range as reported previously (*18*).

The ***h***TBP_{wt}−DNA_{AdMLP} interaction energetics were obtained by partially saturating the labeled DNA with ***h***TBP_{wt} and then monitoring the steady-state fluorescence as the temperature was varied, using protein concentrations near the K_d. Twenty nanomolar T*AdMLP$_{dpx}$*F was equilibrated at 20, 15, or 10 °C and the fluorescence spectrum collected from 502 to 625 nm. ***h***TBP was added to final concentrations of 10.5, 15, and 23.5 nM in separate experiments at each temperature and the spectrum obtained following equilibration. The temperature was then decreased by 5 °C (from 20 and 15 °C) or by 10 °C (from 20 °C) and a third equilibrium spectrum obtained. Finally, spectra were collected at each temperature for 20 nM T*AdMLP$_{dpx}$*F saturated with protein. The change in the fluorescein emission intensity was baseline corrected and normalized to the isoemissive point of the spectra of unbound and fully saturated DNA. For each experiment, at both the initial and final temperatures, the ratio of the partial to the maximum fitted amplitude change corresponds to the observed fractional saturation. The calculated association equilibrium constant, K_a, was determined using the relationship:

$$Y^{calc} = \frac{K_a(P_T - Y^{calc}D_T)}{1 + K_a(P_T - Y^{calc}D_T)} \quad (1)$$

where P_T and D_T are total active protein and DNA. A van't Hoff analysis was conducted using each of the nine pairs of K_a values.

Association kinetics curves for ***h***TBP_{wt}−DNA_{AdMLP} were obtained using a customized fluorescence stopped flow device as described (*15, 16, 18*) at 10, 15, and 20 °C with 10−20 nM T*AdMLP$_{dpx}$*F and ***h***TBP_{wt} concentrations from 8.7 to 166 nM, monitoring FRET-derived changes in the fluorescein emission as the DNA population shifted from unbound to ***h***TBP bound. Thirty-nine independent curves were collected, baseline corrected, fit to triexponential decay, and corrected for fluorescein photobleaching, with replicate curves averaged prior to global analysis, all as detailed previously.

The association kinetics were also obtained using anisotropy stopped flow, following the time course of changes in the rotational mobility of the TAMRA as 20 nM T*AdMLP$_{dpx}$ bound to 89.2 nM ***h***TBP_{wt}. These measurements utilized a half-wave plate to rotate the polarization plane of the laser beam incident on the stopped-flow cuvette, followed by a photoelastic modulator (Hinds International, Inc., Hillsboro, OR) with the axis oriented 45° to the E vector of light and modulated at 50 kHz for half-wave modulation. The demodulation circuitry time constant was 1 ms, comparable to the dead time of the stopped flow device and sufficient to detect a second-order rate constant of at least 6 × 10^9 M^{-1} s^{-1}. The demodulator circuitry provided a DC signal and a rectified AC signal, yielding differing functions of the anisotropy as a function of time, $r(t)$, and the time-dependent total fluorescence, $F(t)$. These two quantities could thus be obtained from the appropriate theoretical expressions. In the present case, $F(t)$ was found to be a constant, thus simplifying the sum rule so that $r(t) = \sum r_i \Phi_i(t)$, where Φ_i is the mole fraction of a fluorescent species and r_i is the corresponding anisotropy. $r(t)$ thus tracks the bimolecular association kinetics.

The ***h***TBP_{wt}−DNA_{AdMLP} relaxation constant, R, was determined by challenging the equilibrated ***h***TBP_{wt}−T*AdMLP$_{dpx}$*F complex with a large excess of unlabeled AdMLP$_{dpx}$ as described (*15, 16*). The subsequent replacement process, as one equilibrium state relaxed to another, was monitored by measuring the time-dependent change in the steady-state fluorescence as $DNA_{unlabeled}$ replaced $DNA_{labeled}$. Briefly, 20 nM ***h***TBP_{wt}−T*AdMLP$_{dpx}$*F was challenged with ∼500 nM, 1 μM, or 2 μM unlabeled AdMLP$_{dpx}$ at 10, 15, and 20 °C. The composite curve constructed from the three to six replicate curves obtained at each condition was fit to mono-, bi-, and triexponential decay models. Agreement between the thermodynamic data and the association and relaxation kinetics data was evaluated by comparing the amplitude change for each set of kinetics curves with that observed for the equilibrium isotherms.

Discrimination among Possible Mechanistic Models. That ***h***TBP−DNA_{AdMLP} recognition proceeds through multiple steps was revealed directly by two of the observed interaction characteristics: neither the biphasicity of the association kinetics nor the inverted temperature dependence of the relaxation kinetics can derive from a single step reaction; an explanation for the latter is included in the Supporting Information. The simplest reaction model could thus be eliminated independently of model fitting.

The ability of a two-step, single intermediate model to accommodate the data ensemble was then evaluated using a set of three linear relationships based on the observed decay constants, or eigenvalues (λ), associated with this model. For cases in which the one-intermediate model is appropriate, these three lines have a common intersection within experimental error; details of this analysis are included in the Supporting Information. The lack of such a point for these lines constructed using 15 °C data eliminated this model from further consideration (Figure 1 in Supporting Information).

Global Analysis. The global analysis was thus conducted using the simplest three-step model as follows:

$$\boldsymbol{h}\text{TBP} + \text{AdMLP} \underset{k_2}{\overset{k_1}{\rightleftharpoons}} (\boldsymbol{h}\text{TBP} - \text{AdMLP})_{I_1} \underset{k_4}{\overset{k_3}{\rightleftharpoons}} (\boldsymbol{h}\text{TBP} - \text{AdMLP})_{I_2} \underset{k_6}{\overset{k_5}{\rightleftharpoons}} \boldsymbol{h}\text{TBP} - \text{AdMLP}_{final} \quad (2)$$

where I_1 and I_2 are discrete conformers of the protein−DNA complex. The fitted parameters were the values for the six rate constants at 20 °C and their corresponding activation enthalpies together with the quantum yield values for the

three bound duplexes relative to that of the free duplex. The reliable extraction of 15 parameters from this analysis has been demonstrated (*15, 16, 18*) and is detailed in the Supporting Information. Values for the successive changes in entropy and free energy were obtained by the application of transition state theory. This comprehensive analysis of the combined thermodynamic and association and relaxation kinetics data adhered to the methods developed previously for the ***y***$TBP_{wt}-DNA_{TATA}$ reaction (*15, 16, 18*). The rigor of the analysis was augmented by requiring agreement between the observed amplitude changes for the stopped flow association and equilibrium data. Additionally, the measured rate constants had to be consistent with the K_a values and also combine with the relative quantum yields to give the correct amplitude changes. Because the fitting procedure is described in detail in the above referenced publications, only those aspects of the analysis unique to this study are elaborated below.

The data ensemble comprised seven averaged stopped flow kinetic curves and the K_a and R values determined at each of the three temperatures. Each association kinetics curve was represented by 41 points with the first half corresponding to λ_1 and extending to $5t_{1/2}$ (fast phase), with the remainder corresponding to λ_2 and continuing to the final equilibrium position. The average error in these points was 1.5%. Because these reactions ranged from partial to essentially full completion, the observed overall amplitude changes were incorporated into the analysis as an additional constraint, requiring agreement with the calculated K_a values.

The calculated values for the points describing each theoretical curve were derived from numerical integration using the rate constant matrix for the two-intermediate model (*27*). This matrix and the associated integration routine differed from that used previously because the lower TBP concentrations did not correspond to pseudo-first-order conditions. This procedure gave the concentrations of each species as a function of time. These values together with the relative quantum yields for each species yielded the calculated response function, which relates directly to a given observed kinetics curve. The overall quality of the global fit was determined as described from the reduced χ^2 (σ^2_{global}) value, which was the weighted sum of the reduced χ^2 values for the stopped flow, relaxation, and equilibrium binding curves (*18*). As in previous analyses, the fluorescein quantum yield for each species, relative to that of the unbound duplex, reflected the extent of DNA bending. The quantum yield value for the final complex was constrained by an upper limit of 0.7 but was allowed to vary lower, toward increased bending. The values for I_1 and I_2 were also varied but constrained to have values larger than or equal to the average.

Donor−Acceptor Distance Distributions. Interdye distance distributions, which reflect the degree of protein-induced helical bending, were determined from time-resolved emission decays of single- and double-labeled $AdMLP_{dpx}$ both unbound and ***h***TBP_{wt} bound at 20 °C exactly as described (*5, 14–16, 23, 25, 28*) except that an additional 1 cm path length liquid filter of 24.13 mM acetate-buffered dichromate, pH 4, was placed between the sample and detector to eliminate any traces of excitation light. Briefly, the fluorescein emission for each case was captured in the nanosecond time regime using 10−30 nM duplex DNA and 160−180 nM ***h***TBP. These pairs of emission decay curves for the unbound and bound duplex were analyzed to obtain the corresponding distance distribution parameters, $\bar{R}$ (the mean interdye distance) and σ (the width of the interdye distance distribution), using the method of moments as described (*24*). The parameter values for the bound DNA were obtained by correcting for the small mole fraction of free duplex present in solution (<4%).

RESULTS

h*TBP$_{wt}$−DNA$_{AdMLP}$ Solution Structure.* The average DNA_{AdMLP} bend induced in solution by full-length ***h***TBP_{wt} was determined from time-resolved emission of the FRET donor (Figure 1, panel C). $\bar{R}$ for the unbound duplex was 65.1 ± 0.3 Å (for R_0 = 63.61 Å and τ_D* = 4.12 ns) with σ = 5.3 ± 0.3 Å. The corresponding values for the ***h***TBP_{wt}-bound duplex were $\bar{R}$ = 50.2 ± 0.2 Å and σ = 5.6 ± 0.1 Å. The TBP-induced DNA bend is well described by a simple model incorporating a kink at each end of the TATA box (*5, 14*). Consistent with this model, the change in the mean T*$AdMLP_{dpx}$*F interdye distance upon ***h***TBP binding corresponds to a helical bend of 97°, in general agreement with the value of 102° estimated previously from stopped flow amplitudes (*22*).

h*TBP$_{wt}$−DNA$_{AdMLP}$ Binding and Kinetics.* The ***h***TBP_{wt}-promoter thermodynamics were obtained from a series of nine experiments, each with constant composition but varied temperature, yielding a set of nine overlapping van't Hoff plots, with $\Delta H°$ = 22 ± 1 kcal/mol. The corresponding values of the association equilibrium constant from eq 1 for 10, 15, and 20 °C were 33 ± 6, 66 ± 9, and 132 ± 8 μM^{-1}, respectively. The average total amplitude change at saturating ***h***TBP_{wt} concentrations was −52 ± 3% and was temperature independent.

The most striking aspect of the stopped flow association curves is the rapidity of the initial phase of the reaction (Figure 2, panel A). The overall observed amplitude changes were in excellent agreement with those predicted from the equilibrium constants; for example, the observed changes for 166 and 55 nM TBP were 47 ± 1% and 36.2 ± 0.6%, respectively, compared to the predicted values of 46.7% and 36.9%. Panel B of Figure 2 shows the normalized anisotropy signal as the single-labeled duplex binds ***h***TBP under the same reaction conditions used to obtain the corresponding FRET signal in panel A. Notably, the two curves agree within experimental error and yield the same amplitudes and eigenvalues for the two reaction phases (inset). The implications of this agreement between the FRET and anisotropy association signals are considered in the Discussion section.

The ***h***$TBP_{wt}-DNA_{AdMLP}$ relaxation kinetics at all temperatures sampled were very well described by monoexponential decay (Figure 3, solid line). An unexpected temperature dependence was observed: the reaction slows with increasing temperature, with overall half-times for the replacement process of 112, 140, and 166 s at 10, 15, and 20 °C, respectively. As with the stopped flow traces, the observed amplitude changes agreed with the thermodynamic data.

Quantitative ***h****TBP−DNA$_{AdMLP}$ Recognition Mechanism.* The ensemble of ***h***$TBP-DNA_{AdMLP}$ kinetic and thermodynamic data was analyzed globally according to the simplest possible model (eq 2). The reduced χ^2 value for the global fit was 0.88. The rate constants and thermodynamic param-

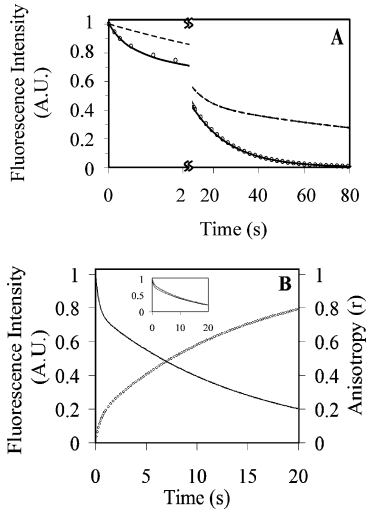

FIGURE 2: Normalized fluorescence stopped flow kinetics curves of ***h***TBP associating with T*AdMLP$_{dpx}$*F (observed, open circles, and calculated, solid line) compared to the corresponding ***y***TBP reaction (broken line, panel A) and in panel B to the ***h***TBP−AdMLP anisotropy stopped flow kinetics trace (open circles). Shown are the time-dependent changes in the donor fluorescein emission as the T*AdMLP$_{dpx}$*F population binds to human and yeast TBP, with the time axis interrupted to clarify the differences (panel A). Although both interactions are biphasic, the human protein binds with an initial relatively very fast phase not seen with the yeast protein and reaches completion significantly faster than does ***y***TBP. Additionally, this fast phase accounts for only 10−22% of the total amplitude change observed with ***h***TBP with these conditions, whereas the faster eigenvalue dominates the ***y***TBP reaction, with the corresponding amplitude ranging from 52% to 75% of the overall change. This difference arises because the equilibrium in the first partial ***h***TBP reaction is strongly toward dissociation, overwhelming the contribution of k_3 and yielding a much less stable complex than with ***y***TBP. The curves shown for both proteins were obtained using 109 nM protein reacting with 20 nM duplex at 15 °C. The ***h***TBP experiments were conducted identically to those using ***y***TBP except for the presence of 10% glycerol in the ***h***TBP buffer, shown previously to have no effect on ***y***TBP kinetics (*22*). The ***y***TBP association curve was constructed for identical conditions using previously collected data (*18*). The ***h***TBP−DNA$_{AdMLP}$ reaction monitored by stopped flow fluorescence anisotropy (open circles, panel B) is compared with the corresponding stopped flow FRET curve (solid line, panel B). The former was obtained using T*AdMLP$_{dpx}$, with the normalized change in anisotropy (r) equal to $(r_t - r_0)/(r_\infty - r_0)$ and is the average of five replicate curves. Both traces are biphasic and show clearly the initial fast phase reflecting $^{h}I_1$ formation. Because the TAMRA emission changes only slightly, the anisotropy change accurately tracks the kinetics of any process yielding a change in rotational correlation time of the labeled oligonucleotide, which in this case is ***h***TBP−DNA$_{AdMLP}$ binding. Replacing the numerator of the above anisotropy expression with $(r_\infty - r_t)$ shows that the two processes are proceeding in tandem (inset), confirming the concurrence of DNA binding and bending. The average signal/noise at $t_{1/2}$ was ∼86 for the FRET data and ∼8 for the anisotropy data; the two curves agree within error.

eters that optimally describe this process are shown in Table 1. The relative quantum yields of $^{h}I_1$, $^{h}I_2$, and the final conformer were 0.52 (0.41, 0.58), 0.52 (0.49, 0.54), and 0.52 (0.48, 0.55), revealing strongly bent DNA in each of these complexes.

DISCUSSION

The present work establishes the protein species specificity of the TBP-promoter interaction with a consensus TATA sequence, with these primary findings: (i) the human protein induces a 97° bend in the *adenovirus* major late promoter compared to 82° with the yeast protein, (ii) human TBP−DNA$_{AdMLP}$ recognition occurs rapidly and concurrently with bending to form a stable ***h***TBP−DNA$_{AdMLP}$ complex in a process that is clearly distinguished from that of the yeast protein, with higher affinity, more rapid binding, and unique intermediate species, and (iii) a quantitative comparison between these two interactions points to the NTDs as the primary regulator of the observed species-specific binding and DNA bending, as discussed below. These results together with previous studies (*5, 14–16, 18, 22*) stipulate the revised paradigm for TBP recognition and deformation of promoter TATA boxes: *both the binding mechanism and the structure of the resulting TBP−DNA complex are dependent on the TATA box sequence and on the TBP species*. The initial view that TBP−DNA$_{TATA}$ structure is independent of these two variables obtains only for crystalline complexes formed with COOH-terminal domains.

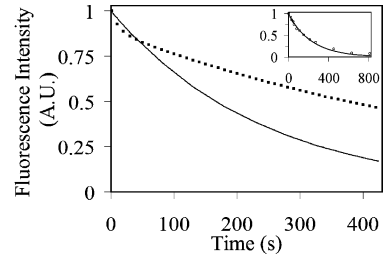

FIGURE 3: Comparative relaxation kinetics of the TBP−T*AdMLP$_{dpx}$*F complex at 20 °C following a challenge with unlabeled duplex for the human (solid line) and yeast (broken line) proteins. The ***h***TBP complex responds to addition of ∼1 μM unlabeled DNA$_{AdMLP}$ with monophasic relaxation with $R = 0.00417$ s^{-1}. In contrast, the ***y***TBP complex yields sharply biphasic decay with $R_1 = 0.0766$ s^{-1} (11%) and $R_2 = 0.00154$ s^{-1} (89%), published previously (*18, 47*). Neither the ***h***TBP nor ***y***TBP (*18*) complex is sensitive to the concentration of challenge DNA from 1 to 10 μM. The full ***h***TBP relaxation curve from the global analysis (solid line) is shown in the inset together with the raw data (open circles). The reaction went to ∼95% completion, and the observed amplitude change was consistent with that from the equilibrium experiments.

Stopped Flow Association Kinetics and Relaxation Kinetics. The most accessible evidence of species-specific function is provided by the association and relaxation kinetics for the human and yeast TBP$_{wt}$−DNA$_{AdMLP}$ reactions. The rapid initial phase of the ***h***TBP reaction proceeds up to 29× faster than that of ***y***TBP under identical conditions (Figure 2). The ***h***TBP−DNA$_{AdMLP}$ replacement reaction was very well described by monoexponential decay at all temperatures sampled in contrast to the two phases observed for ***y***TBP$_{wt}$−DNA$_{AdMLP}$ (Figure 3).

The relaxation constant reflects the rate of DNA dissociation from an equilibrium mixture of all bound species following a challenge with unlabeled DNA. That the observed relaxation kinetics with the human protein are monophasic with no initial rapid phase is consistent with the negligible $^{h}I_1$ equilibrium concentration. In contrast, equilibrated ***y***TBP−DNA$_{AdMLP}$ includes both $^{y}I_1$ and ***y***TBP−DNA$_{final}$ in appreciable concentrations, which is reflected in the biphasic relaxation kinetics: a small amplitude very fast phase followed by a much slower dominant phase with a 0.0017 s^{-1} rate constant from 15 to 30 °C (*18*). The single eigenvalue for the human complex relaxation is temperature dependent and is on average ∼5× faster than

Table 1: Optimal Rate Constants and Corresponding Enthalpy and Entropy Changes for ***h***TBP−DNA_{AdMLP} Partial Reaction Steps in Accord with Eq 2 Together with Relative Quantum Yields for Each of the Three Bound Species

i[a]	k_i (s^{-1})	$\Delta H_i^{\circ\ddagger}$ (kcal mol^{-1})	$\Delta S_i^{\circ\ddagger}$ (cal K^{-1} mol^{-1})[c]
1	5.5 (5.2, 5.6)[b] μM^{-1}	7.4 (6.2, 8.6)	−4.3 (−8.5, −0.3)
2	2.75 (2.6, 3.1)	3.0 (3.0, 4.1)	−48 (−52, −45)
3	0.41 (0.39, 0.43)	9.5 (7.4, 11)	−30 (−37, −23)
4	0.017 (0.013, 0.022)	3.2 (3.0, 4.9)	−58 (−63.5, −52)
5	0.045 (0.025, 0.066)	26 (22, 28)	23 (8.4, 38)
6	0.022 (0.018, 0.026)	9.2 (6.1, 12)	−37 (−47, −26)
QYI_1	0.52 (0.42, 0.59)		
QYI_2	0.52 (0.49, 0.54)		
QY_{final}	0.52 (0.49, 0.54)		

[a] The values shown are at 20 °C and 1 M standard state for each step, i, along the reaction pathway. The assumption was made that $\Delta C_p^{\ddagger} = 0$; therefore, there is no temperature dependence for $\Delta H_i^{\circ\ddagger}$ or $\Delta S_i^{\circ\ddagger}$. [b] Parameter errors, which derive from a joint confidence region, were obtained in the following manner: the 15 × 15 variance matrix was calculated from the inverse of the approximate Hessian matrix following the method of Bard (*44*), using a 1% change in the various parameters to calculate the required partial derivatives. The partial derivatives were taken over 50 time points for each of the 10 kinetic curves and over 50 fractional saturation points for each of the 3 binding curves. In other studies, we have used simulated noisy data with appropriately scaled random noise that corresponded to the experimental errors to obtain the distribution of fitted parameters, a widely recommended and common procedure (*45*). That approach yields results that are in excellent agreement with a third approach: knowing the global optimum from 25 random starting positions in parameter space, the 25 sets of parameter values obtained when the Simplex search crossed the 68% joint confidence boundary were used to obtain the distribution of parameter values. The latter two procedures provided estimates that were not dependent on an assumed hyperelliptical joint confidence region. The reported parameter error estimates are averages of those obtained from the variance matrix and the latter procedure employing the joint confidence boundary. Despite the care taken in determining the error estimates, these values must be considered with caution since they are the extreme limits for each individual parameter as projections of the joint confidence region onto a given parameter axis. Because the volume of the joint confidence region is markedly less than that of the hyperrectangle described by all of the parameter errors (*46*), one cannot assume that any parameter vector with projections jointly within the error estimates provides an adequate description of the data. Rather, the valid values are those that adequately represent the satisfactory fits to the experimental data based on the reduced χ^2 values for the stopped flow and relaxation curves of 0.015 and 0.025 (normalized from 1 to 0) and an average 6% error for the equilibrium constant. [c] $\Delta S_i^{\circ\ddagger}$ values were calculated from k_i and $\Delta H_i^{\circ\ddagger}$ using transition state theory.

that of ***y***TBP−DNA. While both passive replacement and facilitated displacement have been observed for complexes of ***y***TBP with the *adenovirus* E4 promoter sequence (*15*) and for an AdMLP variant sequence (*16*), both ***h***TBP−DNA_{AdMLP} and ***y***TBP−DNA_{AdMLP} relaxation occur through replacement only.

Concurrence of DNA Binding and Bending. Observation of the ***h***TBP stopped flow association curves further indicates that the DNA in $^hI_1$ is already severely bent. The widely separated phases of these curves reflect the dominance of k_1 and k_2 in this part of the reaction. That the first eigenvalue λ_1 (equal to k_1[TBP] + k_2) is TBP concentration independent at each temperature points to the preeminence of k_2, so that the reaction is poised far toward dissociation with very little $^hI_1$ formed for these low TBP concentrations. The fact that we nonetheless observe a significant amplitude decrease in the fluorescein emission intensity (and thus an increase in FRET) specifies qualitatively that $^hI_1$ must be significantly bent. Similar DNA bending among $^hI_1$, $^hI_2$, and the final complex was subsequently confirmed by the relative quantum yield values obtained from the global analysis.

The inseparability of ***h***TBP−DNA_{TATA} binding and bending was demonstrated independently using stopped flow anisotropy and required no *a priori* detailed fitting of the FRET kinetics (Figure 2, panel B). That the measured FRET and anisotropy signals yield the same rates for the two phases first confirms that we are measuring the same process. The amplitude information then provides the key insight: since the anisotropies of all bound forms of the duplex DNA can be assumed to be very similar compared to that of the free duplex, the observed multiphasic progression of the anisotropy change must then reflect initial formation of $^hI_1$ and its subsequent conversion to $^hI_2$ and the final complex. Additionally, the small amplitude of the fast phase must arise from the small mole fraction of $^hI_1$ formed up to that point in the reaction, with the amplitude determined by the large dissociation constant in the first partial reaction. Since the progression of the FRET change overlaps that of the anisotropy change, it necessarily follows that the relative quantum yield of $^hI_1$ must be essentially the same as that of the final equilibrium population comprising all three bound species. Agreement between FRET and anisotropy might arise from binding followed by very rapid (e.g., microseconds) bending or from a rapid equilibrium with a fraction of strongly bent free DNA that then binds as we have previously proposed (*20*). Molecular dynamics simulations reveal that rapid and large amplitude DNA bending can occur in the nanosecond time regime (*29*). Additionally, large-scale motions of the core hinge region revealed by molecular dynamics (*30*) would accommodate the binding of such transiently bent DNA, followed by concerted movement of the protein and DNA toward $^hI_1$, the first detectable intermediate. There is thus no evidence with either human or yeast TBP for a detectable bound form of the DNA that is not bent, precluding binding to unbent DNA with subsequent bending to form a different intermediate species.

Notably, the comparable *S. cerevisiae* analysis also showed concurrent binding and DNA bending (*18*), a finding corroborated by anisotropy stopped flow (R. Delgadillo, unpublished data) and by an elegant single molecule study in which changes in Brownian motion were monitored throughout the recognition process (*31*). The four classes of Brownian motion observed, together with their temporal evolution, strongly supported a linear two-intermediate mechanism with $^yI_2$ structurally similar but less stable than the final state, in agreement with our previously published model (*18*). The initial change in Brownian motion, corresponding to $^yI_1$ formation, was interpreted to indicate less bending in $^yI_1$ than in the subsequent bound forms due to intercalation of only the upstream phenylalanine pair into the TATA box. This interpretation assumes that the observed changes in Brownian motion derived exclusively from changes in the bending of the DNA in the various bound species. However, accumulating evidence for a dynamic NTD that changes position upon DNA binding (*32–36*) suggests an alternate view: the movement of the NTD out of the binding site upon initial association with a corresponding change in the effective molecular volume could likewise alter the observed Brownian motion. We believe that the single molecule results may be providing important insight into the movement of the NTD, with $^yI_1$ already

strongly bent, coupled events for which we now have convincing spectroscopic evidence (J. Whittington and L. J. Parkhurst, unpublished data).

How do $^{h}I_1$, $^{h}I_2$, and the final complex differ? Although the trajectory of the DNA through the binding pocket is complex and cannot be easily described by a simple model, certain features provide insight. The DNA up- and downstream of the two phenylalanine sites has B DNA structure. The distortion between these sites can be characterized by three 70−80° angles: the two Phe-induced bend angles, with respect to the vector connecting the Phe pairs, and the dihedral angle that describes the noncoplanar orientation of the entering and exiting B DNA segments. The distance between the two Phe pairs is considerably greater than that between six B DNA bases. To accommodate this increased distance while maintaining base pairing, the DNA is significantly unwound throughout this region. We hypothesize that the three species derive from different degrees of Phe insertion coupled to protein movement in the hinge region (*30*), which is in turn modulated by changes in the NTD position relative to that of the core domain. Such differences would result in coupled changes in the three angles and in unwinding, which cannot be further distinguished with the present data.

Global Analysis Using the Two-Intermediate Model. Global analysis yields an energetic profile showing that each step of the ***h***TBP−DNA_{AdMLP} pathway follows a very similar thermodynamic pattern, with entropy driving successive endothermic transformations in a series of partial reactions that differ markedly from those of ***y***TBP (Figure 4). Coupling these energetics with the corresponding kinetics yields the time evolution of the two proteins' reactions and highlights their differences (Figure 5). The final complex is formed nearly 2 orders of magnitude faster with ***h***TBP than with ***y***TBP. $^{y}I_1$ remains at high mole fraction far longer than $^{h}I_1$ and is still present at equilibrium at significant population. In contrast, $^{h}I_1$ drops off within the first second over our range of conditions and is negligible at equilibrium at 37 °C. Notably, $^{h}I_2$ builds as high as 0.66 mol fraction at 15 °C, due to the greater stability of $^{h}I_2$ over $^{h}I_1$ and the much larger k_3 value relative to k_4 and k_5. $^{y}I_2$ is significantly *less* stable than $^{y}I_1$, with the corresponding rate constants leading to rapid depletion rather than accumulation. The 2.7 kcal mol^{-1} lower free energy of $^{h}I_2$ compared to $^{y}I_2$ underscores this difference (Figure 4). While an I_2 species was absolutely required to accommodate the collective ***y***TBP−DNA_{AdMLP} data (*18*), its maximum mole fraction was ≤0.09 at any sampled temperature. Thus, whereas both proteins form multiple discrete TBP−DNA conformers at equilibrium, I_2 dominates the ***h***TBP reaction but I_1 dominates with ***y***TBP. Under optimal *in vivo* conditions, $^{h}I_2$ becomes negligible at equilibrium while $^{y}I_1$ constitutes 0.16 of the equilibrated mixture of bound complexes.

Kinetic vs Thermodynamic Control of TBP−DNA Binding. An intermediate ***y***TBP−DNA_{TATA} species has been proposed as the biologically relevant complex to which subsequent transcription factors and regulatory proteins preferentially bind (*18*), a hypothesis supported by a growing body of evidence (*15, 16*). To begin exploring this model for the ***h***TBP−DNA_{AdMLP} interaction, simulations of PIC assembly were conducted as described (*18*), utilizing eq 2 and the globally determined microscopic rate constants at 37 °C.

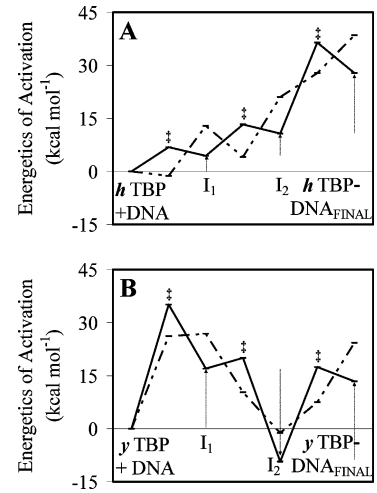

FIGURE 4: The energetic progression of the reaction from TBP + DNA_{AdMLP} on the left to the most stable binary complex on the right for the human (A) and yeast (B) proteins at 25 °C. Differences in the energetics of the ***h***TBP and ***y***TBP (*18*) reaction progressions are readily apparent from a graphic representation of $\Delta H^{\circ\ddagger}$ (solid line) and $T\Delta S^{\circ\ddagger}$ (dashed line). Both reactions are endothermic overall, with ΔH° and ΔS° values for ***h***TBP of 27.8 (23.8, 31.8) kcal mol^{-1} and 131.3 (118, 145) cal K^{-1} mol^{-1} and for ***y***TBP, 13.4 (11.6, 15.2) kcal mol^{-1} and 81.3 (76.6, 86.6) cal K^{-1} mol^{-1} (*18*). These "overall" values represent the difference between the thermodynamic parameters for the final complex and free TBP + DNA. Because all three conformers are present at equilibrium, the observed change in such parameters is the difference between a weighted average of the three bound species and the corresponding value for the reactants; ΔH° obtained from the van't Hoff analysis thus differs from the "overall" value shown in the figure [Table 1 (*18*)]. The modest activation energy of 7 kcal mol^{-1} required for the first ***h***TBP transition (TBP + $DNA_{AdMLP} \rightarrow I_1$) differs markedly from that of the ***y***TBP pathway, for which this step presents the largest energetic barrier with $\Delta H^{\circ\ddagger} = 35.1$ kcal mol^{-1}. The latter is overcome by a commensurate increase in entropy with $\Delta S^{\circ\ddagger} =$ 87.8 cal K^{-1} mol^{-1}, in contrast to the *decrease* in entropy in the course of $^{h}I_1$ formation with $\Delta S^{\circ\ddagger} = -4$ cal K^{-1} mol^{-1}. In the second partial reaction ($I_1 \rightarrow I_2$) the ***h***TBP transformation repeats its pattern for the first step with a similar entropic gain and enthalpic loss. In contrast, the ***y***TBP partial reaction is strongly exothermic with a decrease in entropy, with $\Delta H^{\circ\ddagger} = 3$ kcal mol^{-1} and $\Delta S^{\circ\ddagger} =$ −55 cal K^{-1} mol^{-1}. The result is that, whereas the $^{h}I_2$ conformer is 6.3 kcal mol^{-1} higher in energy and 27.9 cal K^{-1} mol^{-1} higher in entropy than $^{h}I_1$, the corresponding thermodynamic changes in the ***y***TBP reaction are −26 kcal mol^{-1} and −94 cal K^{-1} mol^{-1}, respectively. In the final transformation, $^{h}I_2$ surmounts a substantial activation energy to become ***h***TBP−$AdMLP_{final}$, aided by an accompanying increase in entropy, with $\Delta H^{\circ\ddagger} = 25.7$ kcal mol^{-1} and $\Delta S^{\circ\ddagger} = 23.1$ cal K^{-1} mol^{-1}, to achieve the largest energetic changes, with ΔH° and ΔS° values of 17.1 kcal mol^{-1} and 59.6 cal K^{-1} mol^{-1}. The final ***y***TBP step is likewise entropically driven as the energetic losses associated with $^{y}I_2$ formation are overcome to form the final complex. The largest partial free energy change for ***h***TBP, −8.7 kcal mol^{-1}, occurs in the initial binding step. $^{h}I_2$ is 2.0 kcal mol^{-1} lower in free energy than $^{h}I_1$ whereas $^{y}I_2$ is significantly less stable than $^{y}I_1$. The corresponding equilibrium constant is thus 100× larger for the complex incorporating the human protein. Transition states are denoted (‡), and arrows show progressive changes in ΔH°.

hTBP, DNA, and TFIIA concentrations were set at 10 μM, near the presumed nuclear concentrations, and the rate constant for TFIIA binding to all ***h***TBP−DNA complexes was 3.7×10^6 M^{-1} s^{-1}, determined by direct measurements in our laboratory using ***y***TBP (*37*), followed by rapid PIC formation. With thermodynamic control of the reaction, PIC assembly can occur only from ***h***TBP−DNA_{final}. With kinetic control $^{h}I_1$, $^{h}I_2$, and the final complex are all potential targets

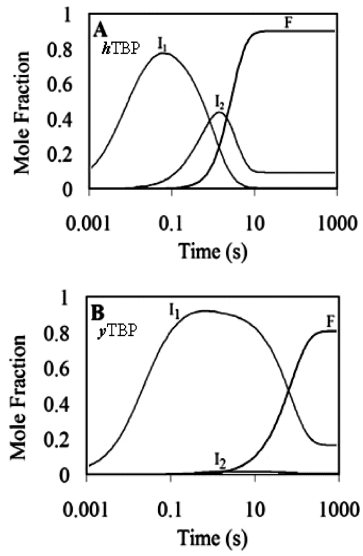

FIGURE 5: Comparison of the mole fractions of the ***h***TBP and ***y***TBP species at optimal *in vivo* temperatures. The time-dependent populations of the three TBP−DNA_{AdMLP} species formed during association with the human protein at 37 °C (A) and the yeast protein at 30 °C (B) were simulated using 10 μM DNA_{AdMLP} and 10 μM protein and previously collected ***y***TBP data (*18*). The species-dependent differences are apparent in the rates of complex formation overall and in the comparative evolution of I_1, I_2, and the final conformer (F) for each protein.

for nucleating PIC assembly, and the fully bent DNA_{AdMLP} in all three complexes renders them transcriptionally active conformers. Notably, however, the large populations of $^hI_1$ and $^hI_2$ result in little formation of the ternary complex from the final conformer with kinetic control of the process. Simulations show that such kinetic control yields a half-time of 0.14 s for PIC assembly, nearly ~145× faster than with thermodynamic control, with >98% of the PIC assembling on the intermediates rather than on the thermodynamically most stable species.

Correlation of TBP-Induced Bend Angles and Transcription Activity. The extent of ***y***TBP-induced TATA box bending is strongly correlated with both *in vitro* and *in vivo* transcription activity (*5*). We therefore asked whether this relationship is general or TBP species specific. Indeed, the more severe induced bend angle (Figure 6) and higher transcription activity of ***h***TBP (*38*) relative to ***y***TBP sustain this correlation (Figure 7). This broadened range of bend angles is a particularly important observation since it is the first evidence that the DNA bends induced by TBP are "universally" a basic determinant of the efficiency of transcription activation. The *adenovirus*, which infects humans, appears to have evolved its promoter to favor the human transcription machinery with a TATA box maximally bent by the human TBP to effect maximum transcription activity. Preliminary studies in our laboratory suggest that, as with ***y***TBP, the TATA box bends induced by ***h***TBP are TATA sequence dependent (J. Whittington, unpublished data), and we expect that this structural variability will likewise correspond to variable transcription rates. Variable promoter bending has been proposed to mediate differential binding and affinities of subsequent transcription factors, particularly TFIIA and TFIIB (*5*).

*NH_2-Terminal Domains Apparently Specify Differences between **h**TBP and **y**TBP.* What is the source of structural and functional differences observed when ***h***TBP_{wt} or ***y***TBP_{wt}

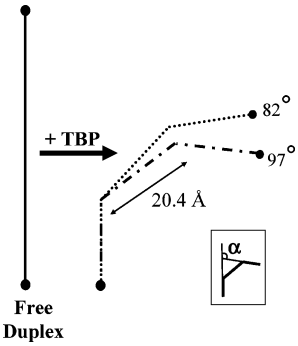

FIGURE 6: Comparative T*$AdMLP_{dpx}$*F bending by ***y***TBP_{wt} (dotted line) and ***h***TBP_{wt} (broken line). Time-resolved FRET provides a rigorous approach to the determination of the structure of TBP−DNA_{TATA} complexes in solution, yielding emission decays from which the probability distribution of the 5′TAMRA−3′fluorescein distance can be precisely determined (*5, 14–16, 23, 24*). Further, the sensitivity of measurements at ~60 Å with this dye pair is such that a 1° change in the bend angle results in a 1% change in the observed emission intensity. A high degree of confidence is thus ascribed to the difference measured for the ***h***TBP and ***y***TBP induced bends, with the latter redetermined herein under identical conditions using ***y***TBP prepared as described (*22*). ***y***TBP-bound T*$AdMLP_{dpx}$*F has an $R = 52.2$ Å with $\sigma = 8.9$ Å. Bend angles (α) were obtained from these data using a simple two-kink bending model (*5, 14*) and the method of moments (*24*).

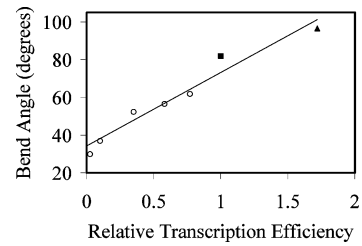

FIGURE 7: *In vitro* transcription efficiency (*38*) is strongly correlated with the degree of the TBP-induced bend for both the human and yeast proteins. Experimentally measured bends induced by ***y***TBP in AdMLP (solid square) and the A3, T6, C7, G6, and T5 AdMLP variant TATA sequences (open circles in order from bottom left) have been shown previously to correlate with both *in vitro* and *in vivo* transcription activity (*5*). The high relative transcription activity of ***h***TBP−DNA_{AdMLP}, 172% (*38*), and the mean ***h***TBP-induced AdMLP bend angle of 97° (solid triangle) extend this trend ($R^2 = 0.957$). The ***y***TBP−DNA_{AdMLP} bend angle was redetermined herein to ensure comparability.

react with the AdMLP TATA box? Experiments were carefully performed to ensure that the only variable was the TBP species. The observed variations must therefore arise from differences in the two proteins. The COOH-terminal domains of yeast and human TBP are 81% homologous (*8*) with nearly 100% conservation of the contact residues (*7, 8*). Although the dissimilarities in DNA bending and recognition could conceivably arise from the noncontacting nonconserved residues within the core domain, the invariance of the X-ray structures and minor changes in the protein core upon DNA binding (*6, 9*) argue against this view.

In contrast to the core domains, the NH_2-terminal domains vary dramatically among TBP species, with only 17 conserved residues between the yeast and human domains and with an additional 99 residues in the ***h***TBP domain. The present results are consistent with previous observations that evolutionarily divergent NTDs confer species specificity to transcription processes (e.g., refs *39–43*). ***y**TBP-promoter binding appears to be regulated by NTD occupancy of the*

concave binding saddle and requires NTD movement away from this site toward the convex surface of the DNA binding domain, creating a two-domain interaction surface for subsequent binding of other transcription and regulatory proteins (32–36). Although corresponding ***h****TBP studies have not yet been performed, the dissimilarities between the human and yeast domains stipulate substantially different architectures for these two NTDs, both with and without bound* DNA_{TATA}*. Notably, this perspective is supported by the markedly higher activation energy for* I_1 *formation with* ***y****TBP (35 kcal* mol^{-1}*) than with* ***h****TBP (7 kcal* mol^{-1}*), consistent with differential NTD occupancy of the DNA binding site. In this view, the highly homologous CTDs are the source of the broad consistency observed in the* ***h****TBP− and* ***y****TBP−*DNA_{AdMLP} *structures and interactions, while the highly variable NTDs impose key modifications of geometry and function to achieve a level of regulatory control.*

ACKNOWLEDGMENT

We are grateful to Professor Michael Brenowitz and Huiyong Cheng for the core TBP, to Dr. Sarah Williams for determining the rate constant for TFIIA binding to ***y***TBP−DNA_{AdMLP}, and to Professor Brenowitz and Professor Mark Griep for critically reading and commenting on the manuscript.

SUPPORTING INFORMATION AVAILABLE

A detailed explanation of the direct evidence for a complex reaction with multiple TBP−DNA species and a discussion of reliably determining 15 parameters using global analysis. This material is available free of charge via the Internet at http://pubs.acs.org.

REFERENCES

1. Hernandez, N. (1993) TBP, a universal eukaryotic transcription factor? *Genes Dev. 7*, 1291–1308.
2. Burley, S. K., and Roeder, R. G. (1996) Biochemistry and structural biology of transcription factor IID (TFIID). *Annu. Rev. Biochem. 65*, 769–799.
3. McKnight, S. L. (1996) Transcription revisited: a commentary on the 1995 Cold Spring Harbor Laboratory meeting, Mechanisms of Eukaryotic Transcription. *Genes Dev. 10*, 367–381.
4. Stargell, L. A., and Struhl, K. (1996) A new class of activation-defective TATA-binding protein mutants: evidence for two steps of transcriptional activation in vivo. *Mol. Cell. Biol. 16*, 4456–4464.
5. Wu, J., Parkhurst, K. M., Powell, R. M., Brenowitz, M., and Parkhurst, L. J. (2001) DNA bends in TATA-binding protein-TATA complexes in solution are DNA sequence-dependent. *J. Biol. Chem. 276*, 14614–14622.
6. Kim, Y., Geiger, J. H., Hahn, S., and Sigler, P. B. (1993) Crystal structure of a yeast TBP/TATA-box complex. *Nature 365*, 512–520.
7. Nikolov, D. B., Chen, H., Halay, E. D., Hoffman, A., Roeder, R. G., and Burley, S. K. (1996) Crystal structure of a human TATA box-binding protein/TATA element complex. *Proc. Natl. Acad. Sci. U.S.A. 93*, 4862–4867.
8. Juo, Z. S., Chiu, T. K., Lieberman, P. M., Baikalov, I., Berk, A. J., and Dickerson, R. E. (1996) How proteins recognize the TATA box. *J. Mol. Biol. 261*, 239–254.
9. Kim, J. L., Nikolov, D. B., and Burley, S. K. (1993) Co-crystal structure of TBP recognizing the minor groove of a TATA element. *Nature 365*, 520–527.
10. Patikoglou, G. A., Kim, J. L., Sun, L., Yang, S. H., Kodadek, T., and Burley, S. K. (1999) TATA element recognition by the TATA box-binding protein has been conserved throughout evolution. *Genes Dev. 13*, 3217–3230.
11. Bleichenbacher, M., Tan, S., and Richmond, T. J. (2003) Novel interactions between the components of human and yeast TFIIA/TBP/DNA complexes. *J. Mol. Biol. 332*, 783–793.
12. Starr, D. B., Hoopes, B. C., and Hawley, D. K. (1995) DNA bending is an important component of site-specific recognition by the TATA binding protein. *J. Mol. Biol. 250*, 434–446.
13. Bernues, J., Carrera, P., and Azorin, F. (1996) TBP binds the transcriptionally inactive TA5 sequence but the resulting complex is not efficiently recognised by TFIIB and TFIIA. *Nucleic Acids Res. 24*, 2950–2958.
14. Wu, J., Parkhurst, K. M., Powell, R. M., and Parkhurst, L. J. (2001) DNA sequence-dependent differences in TATA-binding protein-induced DNA bending in solution are highly sensitive to osmolytes. *J. Biol. Chem. 276*, 14623–14627.
15. Powell, R. M., Parkhurst, K. M., Brenowitz, M., and Parkhurst, L. J. (2001) Marked stepwise differences within a common kinetic mechanism characterize TATA-binding protein interactions with two consensus promoters. *J. Biol. Chem. 276*, 29782–29791.
16. Powell, R. M., Parkhurst, K. M., and Parkhurst, L. J. (2002) Comparison of TATA-binding protein recognition of a variant and consensus DNA promoters. *J. Biol. Chem. 277*, 7776–7784.
17. Strahs, D., Barash, D., Qian, X., and Schlick, T. (2003) Sequence-dependent solution structure and motions of 13 TATA/TBP (TATA-box binding protein) complexes. *Biopolymers 69*, 216–243.
18. Parkhurst, K. M., Richards, R. M., Brenowitz, M., and Parkhurst, L. J. (1999) Intermediate species possessing bent DNA are present along the pathway to formation of a final TBP-TATA complex. *J. Mol. Biol. 289*, 1327–1341.
19. Petri, V., Hsieh, M., and Brenowitz, M. (1995) Thermodynamic and kinetic characterization of the binding of the TATA binding protein to the adenovirus E4 promoter. *Biochemistry 34*, 9977–9984.
20. Parkhurst, K. M., Brenowitz, M., and Parkhurst, L. J. (1996) Simultaneous binding and bending of promoter DNA by the TATA binding protein: real time kinetic measurements. *Biochemistry 35*, 7459–7465.
21. Zhao, X., and Herr, W. (2002) A regulated two-step mechanism of TBP binding to DNA: a solvent-exposed surface of TBP inhibits TATA box recognition. *Cell 108*, 615–627.
22. Masters, K. M., Parkhurst, K. M., Daugherty, M. A., and Parkhurst, L. J. (2003) Native human TATA-binding protein simultaneously binds and bends promoter DNA without a slow isomerization step or TFIIB requirement. *J. Biol. Chem. 278*, 31685–31690.
23. Parkhurst, L. J., Parkhurst, K. M., Powell, R., Wu, J., and Williams, S. (2001) Time-resolved fluorescence resonance energy transfer studies of DNA bending in double-stranded oligonucleotides and in DNA-protein complexes. *Biopolymers 61*, 180–200.
24. Parkhurst, L. J. (2004) Distance parameters derived from time-resolved Forster resonance energy transfer measurements and their use in structural interpretations of thermodynamic quantities associated with protein-DNA interactions. *Methods Enzymol. 379*, 235–262.
25. Williams, S. L., Parkhurst, L. K., and Parkhurst, L. J. (2006) Changes in DNA bending and flexing due to tethered cations detected by fluorescence resonance energy transfer. *Nucleic Acids Res. 34*, 1028–1035.
26. Sjöback, R., Nygren, J., and Kubista, M. (1998) Characterization of fluorescein-oligonucleotide conjugates and measurement of local electrostatic potential. *Biopolymers 46*, 445–453.
27. Zamis, T. M., Parkhurst, L. J., and Gallup, G. A. (1989) A matrix series method for the integration of rate equations in a reaction network. An alternative to Runge-Kutta methods. *Comput. Chem. 13*, 165–171.
28. Hardwidge, P. R., Wu, J., Williams, S. L., Parkhurst, K. M., Parkhurst, L. J., and Maher, L. J. (2002) DNA bending by bZIP charge variants: a unified study using electrophoretic phasing and fluorescence resonance energy transfer. *Biochemistry 41*, 7732–7742.
29. de Souza, O. N., and Ornstein, R. L. (1998) Inherent DNA curvature and flexibility correlate with TATA box functionality. *Biopolymers 46*, 403–415.
30. Miaskiewicz, K., and Ornstein, R. L. (1996) DNA binding by TATA-box binding protein (TBP): a molecular dynamics computational study. *J. Biomol. Struct. Dyn. 13*, 593–600.
31. Tolic-Norrelykke, S. F., Rasmussen, M. B., Pavone, F. S., Berg-Sorensen, K., and Oddershede, L. B. (2006) Stepwise bending of DNA by a single TATA-box binding protein. *Biophys. J. 90*, 3694–3703.

32. Perez-Howard, G. M., Weil, P. A., and Beechem, J. M. (1995) Yeast TATA binding protein interaction with DNA: fluorescence determination of oligomeric state, equilibrium binding, on-rate, and dissociation kinetics. *Biochemistry 34*, 8005–8017.
33. Khrapunov, S., Pastor, N., and Brenowitz, M. (2002) Solution structural studies of the *Saccharomyces cerevisiae* TATA binding protein (TBP). *Biochemistry 41*, 9559–9571.
34. Rashidzadeh, H., Khrapunov, S., Chance, M. R., and Brenowitz, M. (2003) Solution structure and interdomain interactions of the *Saccharomyces cerevisiae* "TATA binding protein" (TBP) probed by radiolytic protein footprinting. *Biochemistry 42*, 3655–3665.
35. Gupta, S., Cheng, H., Mollah, A. K., Jamison, E., Morris, S., Chance, M. R., Khrapunov, S., and Brenowitz, M. (2007) DNA and protein footprinting analysis of the modulation of DNA binding by the N-terminal domain of the *Saccharomyces cerevisiae* TATA binding protein. *Biochemistry 46*, 9886–9898.
36. Khrapunov, S., and Brenowitz, M. (2007) Influence of the N-terminal domain and divalent cations on self-association and DNA binding by the *Saccharomyces cerevisiae* TATA binding protein. *Biochemistry 46*, 4876–4887.
37. Williams, S. L. (2006) Biophysical studies on multiple DNA duplexes and on a protein-protein-DNA transcription complex, Ph.D. Dissertation, University of Nebraska, Lincoln, NE.
38. Wobbe, C. R., and Struhl, K. (1990) Yeast and human TATA-binding proteins have nearly identical DNA sequence requirements for transcription in vitro. *Mol. Cell. Biol. 10*, 3859–3867.
39. Goppelt, A., and Meisterernst, M. (1996) Characterization of the basal inhibitor of class II transcription NC2 from *Saccharomyces cerevisiae*. *Nucleic Acids Res. 24*, 4450–4455.
40. Horikoshi, M., Yamamoto, T., Ohkuma, Y., Weil, P. A., and Roeder, R. G. (1990) Analysis of structure-function relationships of yeast TATA box binding factor TFIID. *Cell 61*, 1171–1178.
41. Kuddus, R., and Schmidt, M. C. (1993) Effect of the non-conserved N-terminus on the DNA binding activity of the yeast TATA binding protein. *Nucleic Acids Res. 21*, 1789–1796.
42. Lee, M., and Struhl, K. (2001) Multiple functions of the nonconserved N-terminal domain of yeast TATA-binding protein. *Genetics 158*, 87–93.
43. Ruppert, S. M., McCulloch, V., Meyer, M., Bautista, C., Falkowski, M., Stunnenberg, H. G., and Hernandez, N. (1996) Monoclonal antibodies directed against the amino-terminal domain of human TBP cross-react with TBP from other species. *Hybridoma 15*, 55–68.
44. Bard, Y. (1974) *Nonlinear parameter estimation*, pp 97, 178 (eqs 5-9-3, 7-15-14, 7-15-15), Academic Press, New York.
45. Press, W. H., Flannery, B. P., Teukolsky, S. A., and Vetterling, W. T. (1989) *Numerical recipes: the art of scientific computing*, pp 529−532, Cambridge University Press, Cambridge, New York.
46. Draper, N. R., and Smith, H. (1998) *Applied regression analysis*, 3rd ed., pp 142−146, Wiley, New York.
47. Powell, R. M. (2001) TATA-binding protein recognition of DNA promoters: kinetics and thermodynamic studies, Ph.D. Dissertation, University of Nebraska, Lincoln, NE.
48. Hague, D. N. (1971) *Fast reactions*, pp 33−37, Wiley-Interscience, New York.

BI800139W